Korean J. Chem. Eng., 33(2), 657-665 (2016)
DOI: 10.1007/s11814-015-0168-x

pISSN: 0256-1115
eISSN: 1975-7220

CO_2/CH_4 separation with poly(4-methyl-1-pentyne) (TPX) based mixed matrix membrane filled with Al_2O_3 nanoparticles

Mohammad Hadi Nematollahi*, Amir Hossein Saeedi Dehaghani,†, and Reza Abedini*****

*Department of Chemical Engineering, Shahreza Branch, Islamic Azad University, Shahreza, Iran
**Petroleum Group, Faculty of Chemical Engineering, Tarbiat Modares University, Tehran, Iran
***Faculty of Chemical Engineering, Babol Noshirvani University of Technology, Babol, Iran
(*Received 11 June 2015 • accepted 30 July 2015*)

Abstract−The effect of alumina (Al_2O_3) nano-particles on gas separation properties of poly(4-methyl-1-pentyne) known as TPX was evaluated. Mixed matrix membranes (MMMs) were prepared with various weight percent (5, 10, 15, 20 and 30) of alumina nano-particles through solution casting along with solvent evaporation method. TPX and consequent MMMs were characterized using FT-IR, SEM and TGA methods. The MMMs permselectivities were determined through pure CO_2 and CH_4 permeation measurement and CO_2/CH_4 selectivity calculation. SEM images demonstrated the proper dispersion of alumina nano-particles in TPX matrix. Results from gas permeation showed that the permeability of both CO_2 and CH_4 as well as CO_2/CH_4 selectivities were increased with increasing alumina content. Significant increase of CO_2 permeability (from 157.43 Barrer at 8 bar and no loading of Al_2O_3 to 527.78 Barrer at 8 bar and 30 wt% loading of Al_2O_3) and conspicuous enhancement of selectivity, from 7.73 to 12.51, were obtained in TPX MMMs.

Keywords: Poly(4-methyl-1-pentyne), TPX, CO_2/CH_4 Separation, Alumina Nano-particles, Mixed Matrix Membranes

INTRODUCTION

Industries continually need to find new strategies to reduce energy consumption, lower investment costs and reduce environmental pollution, so the attitude has shifted to applying membranes in industries such as natural gas sweetening. Over the past decade, this technology, compared to conventional gas separation processes, has had a tremendous growth [1]. The advantages of membrane separation processes such as lower energy requirements, compact structure, lower operating and maintenance cost, ease of processing and also the least impact on the environment caused that membrane technology have increasingly gained interest in various industries [1,2].

Material selection and kind of membranes is the first step in the design of the membrane process. Polymeric membranes are one of the categories used widely nowadays (especially in gas separation), where thermal, chemical and physical properties of the polymer affect significantly the performance of prepared membranes [3]. The improper thermal and mechanical stability of polymeric membranes along with no appropriate selectivity in the operating conditions are the main problems that limit the use of these membranes. Hence, many studies, such as the use of various particles (*i.e.*, metal oxides, carbon nano-tubes, zeolites, MOFs and etc.) in the polymer matrix, have been made to improve the efficiency of the polymeric membranes [4-7]. Nano-particles with high exposure levels and appropriate interaction with the polymer phase that arises from their small size can interact with penetrant gas properly, which results in subsequent higher selectivity and also leads to desirable properties such as good mechanical strength and thermal stability of membranes [8]. These studies introduced new membranes with improved properties known as mixed matrix membranes (MMMs) which have higher separation performance compared to neat polymeric membranes. Based on the use of nano-particles in polymeric membranes to enhance the gases' permeability and selectivity, extensive research has been done in recent years.

Ahn et al. evaluated the gas permeability properties of the polyethersulfone (PES) membrane filled with nanosilica particles. The results showed that the increase of silica content in polymer matrix enhanced the permeability of all gases, and particularly for oxygen and methane, the permeability increased about 4-fold and 5-fold, respectively, compared to the silica-free counterpart. Although the gases' permeability increased, due to selectivity decline the MMMs were not capable to overcome the Robeson upper bound. The disruption of polymer chains due to presence of particles increased the free volume of membranes, and thereby the gases' permeability increased [9].

Valero et al. studied the effect of combined MCM-41 and MOF on gas transport properties of polyimide (PI) and polysulfone (PSf). Prepared MMMs were comprised by 16 wt% of particles and 84 wt% of polymer. The various nanoparticle compositions of the (MCM-MOF) (i.e., (0-16), (4-12), (8-8), (12-4) and (16-0)) were used to prepare MMM: (0-16) means the membrane filled with 16 wt% MOF and (16-0) shows the membranes contain 16 wt% MCM-41. With increasing the MOF loading, the H_2 permeability decreased and H_2/CH_4 selectivity increased. The optimal composition of MMMs

†To whom correspondence should be addressed.
E-mail: asaeedi@modares.ac.ir

was achieved at particles loading of (4-12) and (8-8). The gases' permeability in PSf membranes was greater than PI ones. In spite of permeability, PI membranes showed higher H_2/CH_4 selectivity compared to PSf membranes [10].

Hassanajili et al. evaluated the separation of CO_2/CH_4 in polyester polyurethane (ESPU) and polyether polyurethane (ETPU) membranes filled with silica particles. Permeation tests showed that the permeability increased and CO_2/CH_4 selectivity enhanced with increasing silica content. Results demonstrated that solubility affected gases' permeability in neat membrane, whereas for MMMs, both solubility and diffusivity showed significant influence on gases' permeability. At pressure of 10 bar, the ESPU membrane containing 15 wt% of silica showed a CO_2 permeability and CO_2/CH_4 selectivity of 12 Barrer and 35.4, respectively. At the same condition, ETPU with 15 wt% of silica revealed a permeability of 8.9 Barrer for CO_2 and a CO_2/CH_4 selectivity of 28.3 [11].

The higher permeability of rubbery polymers as well as higher chemical stability caused most studies to use these polymers for membrane fabrication. But, recent work has introduced a fabricated membrane from glassy polymers which has high selectivity and proper permeability. Generally, rubbery polymers compared to glassy ones have higher permeability which is attributed to their greater chain movement. In spite of high permeability of rubbery polymers, membranes prepared from glassy polymers show higher selectivity.

Acetylene polymers with low density, high free volume and superior gas permeability are used to separate gases widely [12,13]. This category includes poly(1-(trimethylsilyl)-1-propyne) (PTMSP) and poly(1-trimethylgermyl-1-propyne) (PTMGeP). However, low chemical resistance of PTMSP and PTMGeP caused better resistance polymer based on acetylene with polymethylpentene (PMP) with high gas permeability among the polymers to be employed for membrane gas separation [13,14].

He et al. examined mixed matrix membranes comprised of poly (4-methyl-1-pentyne) (PMP) and silica particles in separation of n-C_4H_{10}/CH_4. Their results showed that pure PMP membrane reveals different gas permeation property compared to PMP/silica mixed matrix. The increasing in the embedded silica loading in the PMP polymer matrix resulted in gas permeability and n-C_4H_{10}/CH_4 selectivity enhancement. n-C_4H_{10}/CH_4 selectivity was 13 for the pure PMP while the value of selectivity for the PMP filled with 45 wt% of silica increased to 26. In addition, the permeability of n-C_4H_{10} increased 3 to 4 times compared to neat PMP [15].

Abedini et al. studied the effects of MIL 53 particles on PMP MMMs to separate and purify hydrogen based on the reverse selectivity. The solubility of CO_2 compared to hydrogen has been increased significantly with increasing the MIL53 particle in PMP matrix. Rising feed pressure and embedding of nano-particles causes the permeability of CO_2 as well as CO_2/H_2 selectivity to increase [16].

In another study Abedini et al. examined the effects of functionalized NH_2-MIL 53 particles on the properties of PMP in the separation of CO_2/CH_4. Results showed an increase in the permeability of CO_2 as particle loading increased in the polymer matrix. Moreover CO_2/CH_4 selectivity was increased significantly [17].

With regard to the above, PMP was used to attain more permeability in gas separation studies. Poly(4-methyl-1-pentyne), known as TPX, is a polyolefin quasi-crystalline with properties such as high free volume as well as high gas permeability, good thermal stability and chemical resistance, high initial decomposition temperature and low density [18-20]. In fact, among the known polymers in gas separation processes, PMP has the superior permeability of pure hydrocarbons [12], so that PMP is introduced as a proper material to fabricate dense homogeneous membranes for gas separation.

The purpose of this study was to fabricate a mixed matrix membrane with high free volume through adding inorganic nanoparticles to polymer matrix. Hence TPX was used as a membrane matrix (the dominant phase) and the alumina nanoparticles as an additive. For characterization of fabricated membranes, Fourier transform infrared spectroscopy (FT-IR), thermal gravimetric analysis (TGA) and scanning electron microscopy (SEM) have been used. The gas separation properties of comprised mixed matrix membranes were evaluated through pure CO_2 and CH_4 permeation as well as CO_2/CH_4 selectivity calculation. In addition, the effect of feed pressure on each gas permeability and CO_2/CH_4 selectivity was measured.

MATERIALS AND METHODS

1. Material

The low molecular weight poly(4-methyl-1-pentyne) or TPX as a polymer phase of membrane was purchased from Sigma-Aldrich Co., USA. Alumina (Al_2O_3) nanoparticles used as a dispersed phase and purchased from Merck Co. and carbon tetrachloride (CCl_4) as a solvent of the polymer with 99.8% purity were supplied by Merck Co., Germany.

2. Preparation of Membranes

To prepare membranes, at first, TPX polymer was placed in a vacuum oven at 60 °C for 6 h to remove any possible moisture. Neat TPX membrane was prepared by dissolving 3 wt% of TPX in CCl_4 for 24 h. For MMMs, the membrane preparation process was similar to neat TPX with the previous step, which consisted of the alumina distribution in CCl_4. Alumina nanoparticles were dispersed in CCl_4 solvent under stirring for 6 h, and to obtain a uniform particle distribution in the solvent, a suspension comprised of solvent and alumina was sonicated for 10 min. Then, TPX was added to the mixture and dissolved in solvent for h 24 under stirring. The final solution was degassed in the oven at room temperature and for 6 h. The bubble removed solution was cast on a smooth and flat Teflon plate to evaporate the solvent of the cast film. To slow evaporation of CCl_4 and prevent any defect during the membrane formation process, a small glassy dish was put over the cast film for 24 h; for further solvent evaporation, the membranes were placed in the vacuum oven at 60 °C for 6 hr. Table 1 shows the composition of each casted solution.

3. Characterization Methods

To investigate the formatted bond and change in MMMs network, FTIR spectroscopy using an Equinox 55 in the range of 400-4,000 cm^{-1} was performed. Each spectrum was taken at an incidence angle of 455 with 30 scans at a wave number resolution of 5 cm^{-1}.

Changes in the cross sectional and surface layers of the mem-

Table 1. Solution composition of neat TPX and each MMM

Membrane	Polymer (5 wt%)		Solvent (wt%)
	TPX	Al_2O_3	CCl_4
TPX	100	0	95
TPX5	95	5	
TPX10	90	10	
TPX15	85	15	
TPX20	80	20	
TPX30	70	30	

brane due to the presence of alumina nano-particles in the polymer matrix as well as the quality of nano-particles dispersion were evaluated through scanning electron microscope (SEM) (KYKY-EM3200, KYKY technology development Ltd., Beijing, China). First membranes were immersed in liquid nitrogen for clean and unfailed cut and then a golden layer was coated on the membranes.

Thermal stability and decomposition temperature (T_d) of neat TPX and MMMs were evaluated by thermal gravimetric analysis (TGA-50, Shimadzu). The desired 10 mg sample of each membrane was pre-heated above 100 °C to remove moisture. Then, the cooled samples were reheated from 20-800 °C under dried and high pure nitrogen gas flow with the rate of 10 °C/min.

4. Permeation Test

A constant pressure system was used to measure the permeability of both CO_2 and CH_4 gases through neat TPX and MMMs. The following equation was used to calculate the permeability:

$$P = \frac{QL}{(P_1 - P_2)A} \quad (1)$$

where P is the gas permeability of the polymer in Barrer (1 Barrer $=10^{-10}$ cm^3 (STP)·cm/cm^2·S·cmHg)) Q is the permeate gas flow (cm^3 (STP)/s), L is membrane thickness (cm), A is the effective membrane surface area (cm^2) and finally P_1 and P_2 are the gas pressure of upstream and downstream, respectively.

The calculation of CO_2/CH_4 selectivity for neat TPX and MMMs was performed through dividing of gas permeabilities as follows:

$$\alpha_{CO_2/CH_4} = \frac{P_{CO_2}}{P_{CH_4}} \quad (2)$$

RESULTS AND DISCUSSION

1. Membrane Characterization

Fourier transform infrared spectrum of a pure TPX membrane and MMMs are shown in Fig. 1. The FT-IR spectrum of pure alumina shows two strong absorption bands at 450 to 598 cm^{-1}, which represents a group of stretching and bending Al-O. The reported bands in the range of 400-1,000 cm^{-1} correspond to a strong wide bond of γ-alumina [21]. Moreover, the absorption band at 3,445 cm^{-1} of γ-alumina was assigned to O-H group. The O-H stretching adsorption band was reported in the range of 3,200-3,400 cm^{-1} [21].

FT-IR result of the neat TPX membrane represents a methyl group (-CH_3) attached to the polymer chain which was assigned to 2,954 and 2,973 cm^{-1} and also the -CH_3 asymmetric and symmetric stretching modes corresponded to the strong bands at 2,888 and 2,869 cm^{-1}. In addition the side carbon-chain of -CH_2-CH-$(CH_3)_2$ in poly methylene is attached to every second carbon atom; thus, the asymmetric stretching C-H bond in CH_3 is assigned to 2,887, 2,928, 2,949, 2,971 cm^{-1}. The bands at 2,864 cm^{-1} represent a symmetrical C-H bond in -CH_3. The bands at 976, 1,054, 1,063 and 1,102 cm^{-1} represent the stretching vibration of C-C [22].

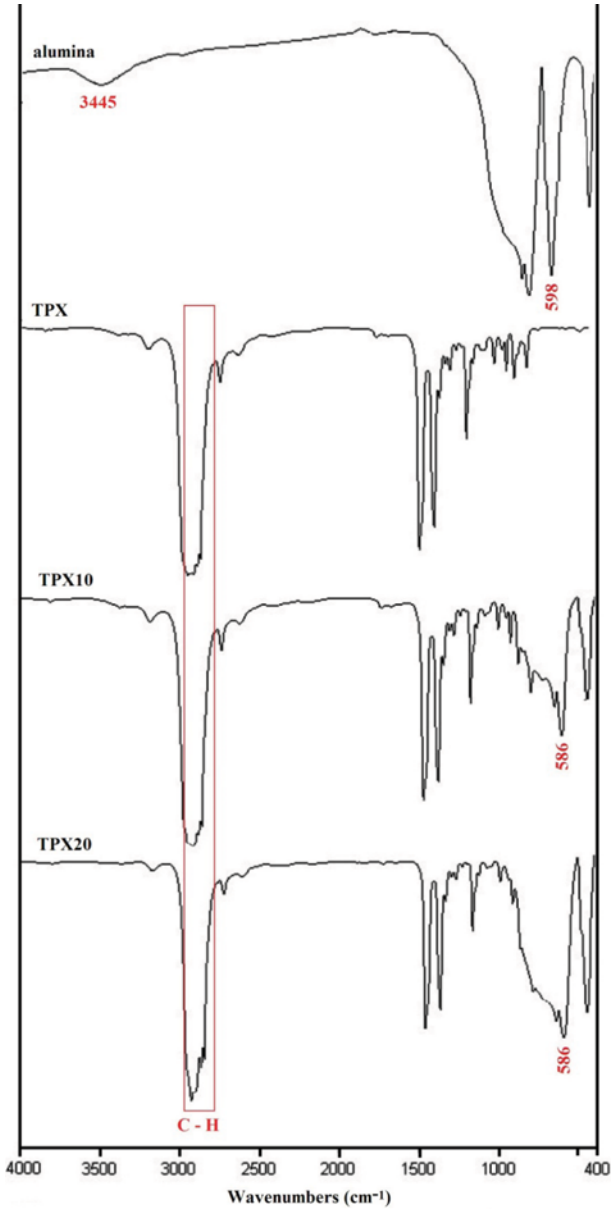

Fig. 1. FTIR spectra of neat TPX and all MMMs.

The TPX filled with alumina nano-particles showed a similar band compared to neat TPX. According to incorporated alumina nanoparticles in the polymer matrix, some shifting existed in spectra of MMMs attributed to the proper interaction between polymer and particles phases. For example, the band at 598 cm^{-1} assigned to Al-O group was shifted to 586 cm^{-1} in MMMs, which reveals the interaction between Al-O and C-H groups.

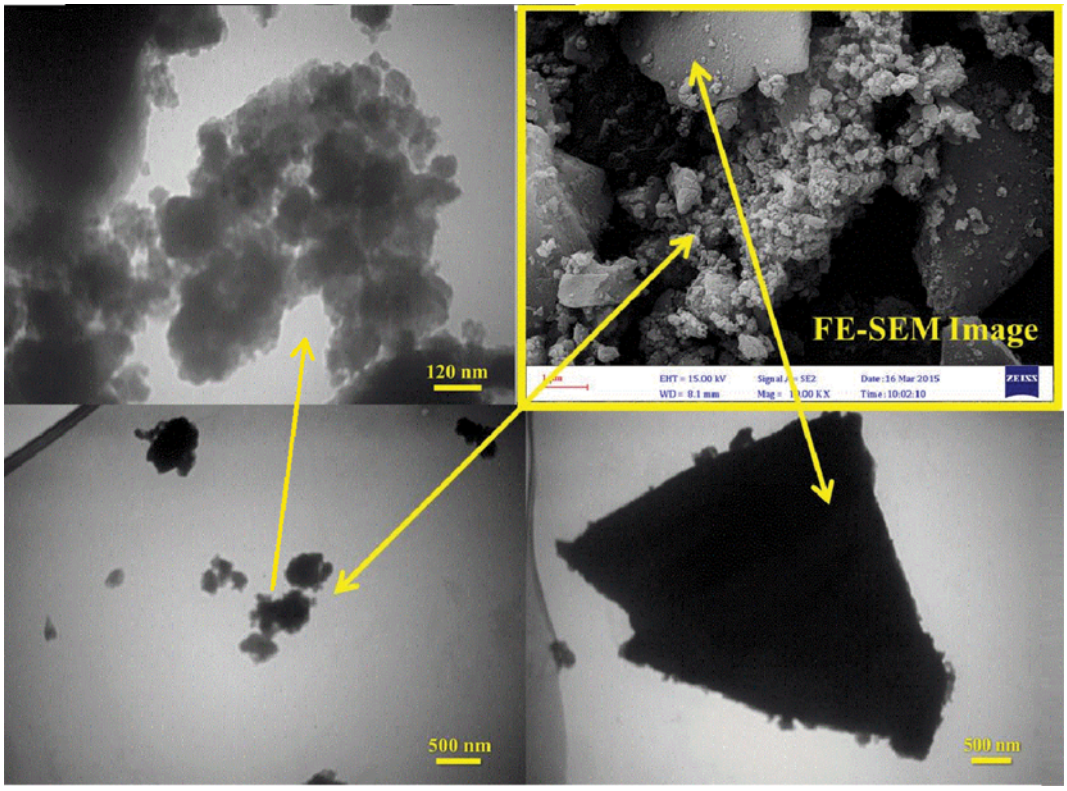

Fig. 2. FE-SEM and TEM images of alumina nanoparticles.

Fig. 2 illustrates the FE-SEM and TEM images of alumina nanoparticles. As shown the alumina particles have size smaller than 100 nm.

Fig. 3 shows the cross-sectional image of neat TPX membrane and MMMs containing 5, 15 and 30 wt% of alumina particles. The SEM image of dense neat TPX membrane (Fig. 3) illustrates a dense consistent structure without any cross sectional imperfection. As can be seen, the cross section structure of MMMs has lost the smooth and integration pattern due to adding of alumina nanoparticles in TPX matrix. The cross section of MMMs illustrates the grooved structure pattern which was raised from the proper compatibility existing between polymer phase and particles, as it is shown in Fig. 3(b)-(d). As shown in Fig. 3, the appearance of grooved-pattern was elongated in cross section of MMMs with increasing the alumina content. The uninterrupted debonding of TPX/alumina crystals due to the intensifying the interfacial stress concentration at higher loading of alumina may lead to this manifestation.

The cross sectional SEM images of the membranes at higher magnification indicated the uniform and appropriate distribution of alumina nanoparticles in a polymer matrix. However, some degrees of alumina agglomeration can be seen. The alumina agglomeration was intensified at higher content of filler (30 wt%).

The thermal stability of alumina nanoparticles and TPX/alumina MMMs was evaluated through TGA method and the results shown in Fig. 4. According to TGA graph, neat TPX demonstrated a proper thermal stability. Fig. 4 depicts that neat TPX showed the thermal degradation temperature (T_d) of 308 °C, which is related to the polymer degradation. For MMMs, the degradation temperature increased significantly to 394 °C. The enhancement of T_d in MMMs induced by presence of alumina nanoparticles can be attributed to the high thermal stability of alumina nano-particles.

2. Permeability and Gas Separation Properties of TPX

To measure the gases' permeability and CO_2/CH_4 selectivity, the constant pressure varying volume system was used. The membrane was held in the permeation cell and the entire permeation setup was placed in an oven. Circular membrane discs with effective permeation area of about 10.75 cm^2 were used for flat sheet gas permeation tests. Gas permeability of neat TPX and all MMMs was calculated at 25 °C and pressure of 4 bar. Effect of feed pressure (2 up to 10 bar) on gas permeation properties of membranes was investigated. The CO_2/CH_4 ideal selectivity of membranes was calculated by dividing the gases' permeability. Table 2 lists the permeability of gases and calculates the corresponding CO_2/CH_4 selectivities of neat TPX and MMMs obtained by taking an average from three replicates.

2-1. Effect of Alumina Loading

As shown in Table 2, gas permeability as well as CO_2/CH_4 selectivity increased by increasing the alumina content in TPX matrix. The CO_2 permeability increased from 129.14 Barrer at no embedded TPX to 325.62 in TPX filled with 30 wt% of alumina. The CO_2/CH_4 selectivity in TPX with 30 wt% of alumina showed 145.4% enhancement respect to the neat TPX. In fact, embedding of different fillers in polymer matrix can affect gas permeation properties of prepared MMMs through these ways:

i) Incorporated fillers elongate the diffusion pathway, which results in lower diffusion of penetrant.

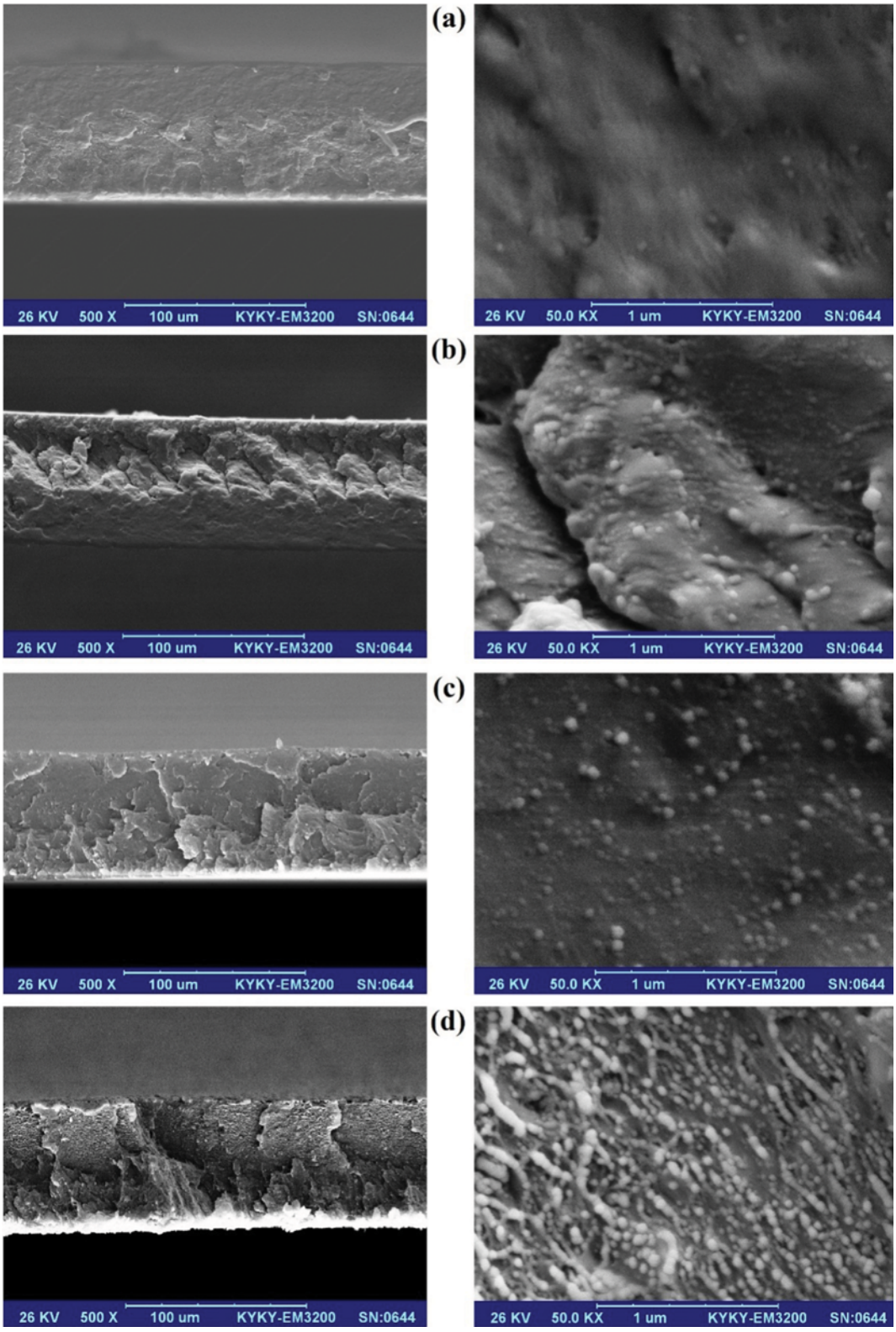

Fig. 3. Cross sectional SEM image of (a) neat TPX, (b) TPX 5, (c) TPX 15, (d) TPX 30.

ii) The free volume of MMMs increases due to presence of fillers resulting in higher gas permeability

iii) Depending on the polymer/filler interfaces, the formation of non-selective voids can enhance the gas permeation.

The CO_2 permeability enhanced more than CH_4 permeability for all membranes. Increasing in free volume of membranes induced

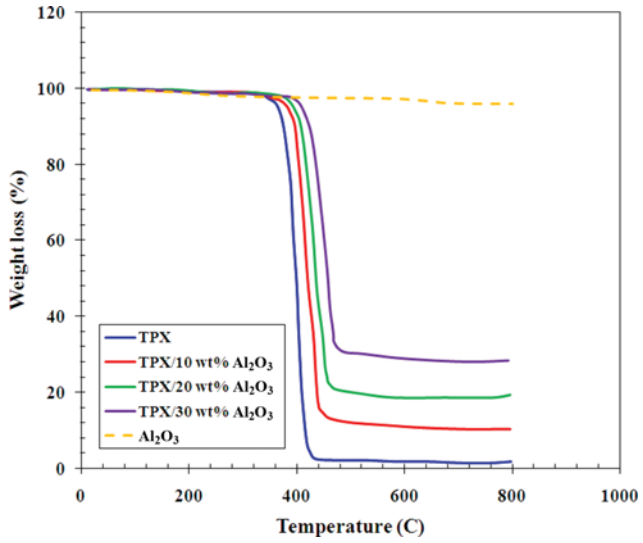

Fig. 4. Thermal gravimetric analysis (TGA) curve of neat TPX and MMMs.

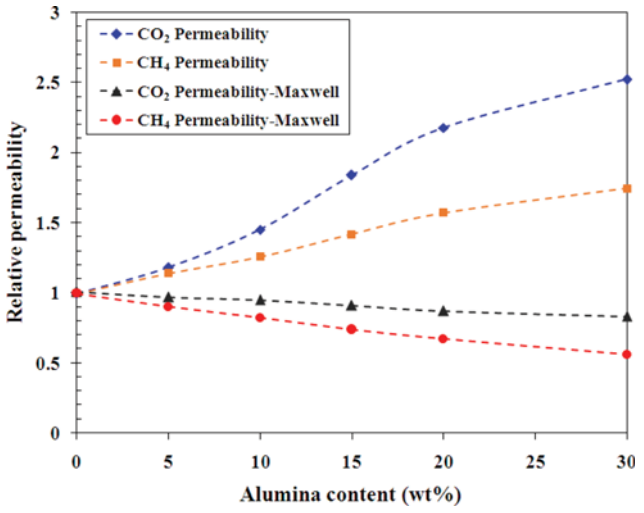

Fig. 5. Increasing in permeability of TPX/alumina mixed matrix membranes to a variety of penetrants as a function of alumina (wt%) at ΔP=4 bar.

Table 2. Gas permeabilities and ideal selectivities of neat TPX and each MMM at 25 °C and 4 bar

Polymer	Permeability (barrer)		CO_2/CH_4
	CO_2	CH_4	
TPX	129.14	16.1	8.02
TPX5	151.1	17.95	8.42
TPX10	185.84	20.31	9.15
TPX15	237.9	23.03	10.33
TPX20	280.67	25.15	11.16
TPX30	325.62	27.95	11.65

by embedded alumina particles resulted in permeability enhancement of both gases. On the other hand, the presence of alumina particles influences the diffusion and solution of gases in MMMs. Diffusion of both penetrants increased by increasing the free volume of MMMs. Consequently, CO_2 with lower kinematic diameter compared to CH_4 diffused more, which resulted in higher permeability. Moreover, more condensability of CO_2 and its interaction with polymer chains increases its solubility besides its diffusivity.

According to Table 2, the highest increment of gas permeability and CO_2/CH_4 selectivity was observed in MMMs with 15 wt% of alumina. This membrane showed an average enhancement of 132% compared to MMM that contains 10 wt% of alumina. The significant increment of permeability and selectivity at alumina loading of 15 wt% can be attributed to the good dispersion of alumina in polymer matrix. SEM images also confirm this behavior where TPX filled with 15 wt% showed the best alumina dispersion within the polymer matrix. In fact, the quality of particle dispersion in polymer matrix is a fundamental parameter to obtain proper separation factor. At lower loading of particles, the less effect from collective effect of interconnected particles which loosely bonded together by van der Waals interactions resulted in lower intensification of particle agglomeration. Hence, the particle agglomerated zones in membrane matrix hinder the gas permeation through MMMs. Although, next to the particle agglomeration which barricades the gas diffusion, the increase in free volume of MMMs as a result of incorporated particles can enhance the gas permeation. Indeed, the trade-off relation between the declared factors should be considered.

Fig. 5 shows a comparison between the permeability of gas data in MMMs with calculated data by the Maxwell model as follows [24].:

$$P_C = P_P\left(\frac{1-\phi_f}{1+0.5\phi_f}\right) \quad (3)$$

where P_C and P_P are the permeability of the MMM and the pure polymer matrix, respectively, and Φ_f is the volume fraction of the nanoparticles.

This model predicts the gas permeability values in mixed matrix membranes are lower than the corresponding values in the pure polymer membranes. In this study the results showed an increase in gas permeability values with an increase in the amount of alumina nanoparticles; while increasing the permeability was incompatible with the prediction of Maxwell model.

This contradiction, based on the Maxwell model, is due to non-porous nano-particles in the membrane matrix that increased the network and the turmoil in the polymer matrix, which leads to reduced permeability coefficient [9]. In addition, the Maxwell model does not consider the interface of polymer and nanoparticles as a separate phase and ignores the interaction between the nanoparticles (nanofillers)-chain polymeric and nanoparticles–penetrating [24].

2-2. Effect of Feed Pressure on MMM Performance

Fig. 6 illustrates the permeability of each gas versus feed pressure increment from 2 to 10 bar for pure TPX and MMMs those containing 5, 15 and 30 wt% of alumina nano-particles. As Fig. 6 shows, increasing the feed pressure caused an increase in the permeability of each gas while the intensity of permeability increased in the 10 bar has declined slightly. According to Fig. 6 permeability of CO_2 in the membrane containing 30 wt% weight of alumina reached the amount of 532.33 Barrer (at pressure of 10 bar) and finally CH_4 reached in the same conditions to 44.04 Barrer. As pres-

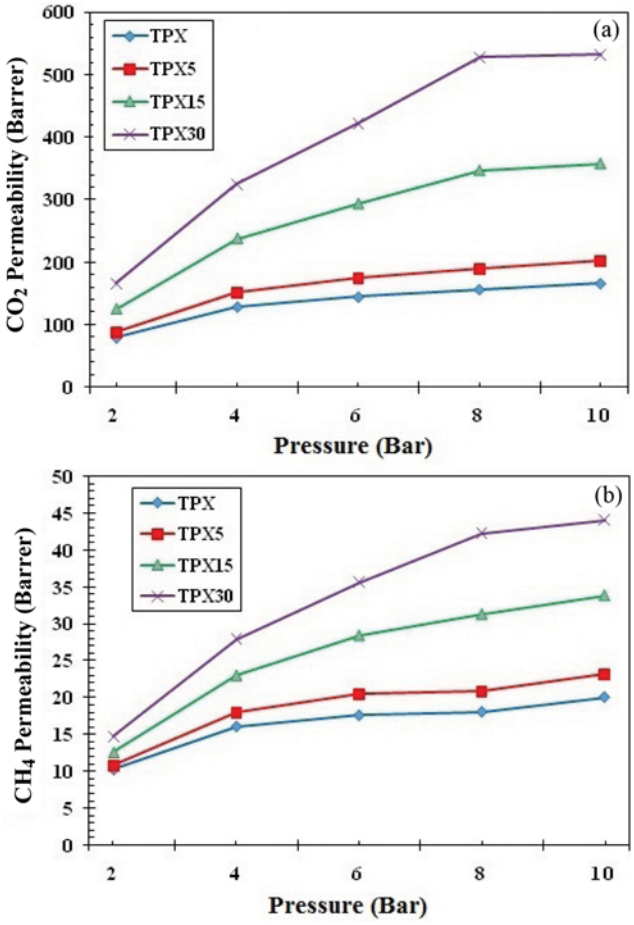

Fig. 6. Effect of feed pressure on permeability of (a) CO_2 and (b) CH_4 for neat TPX and MMMs those containing 5, 15 and 30 wt% of Al_2O_3.

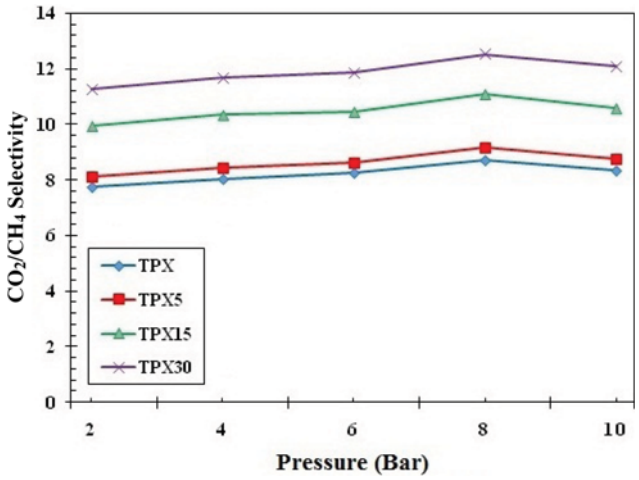

Fig. 7. Effect of feed pressure on CO_2/CH_4 selectivity for neat TPX and MMMs those containing 5, 15 and 30 wt% of Al_2O_3.

sure increases, permeability values of CO_2 compared to CH_4 showed superior growth and no substantially increasing of CH_4 penetration occurred.

Based on dual sorption model (DSM) in glassy polymers, increasing the feed pressure affects the gas permeability as follows:

i) High pressure on feed side of membrane leads to the polymer chain compactness and thereby the fractional free volume (FFV) as well as penetrant diffusion is reduced.

ii) Increasing the feed pressure resulted in increase of condensable gas concentration (i.e., CO_2) which led to polymer plasticization enhancement.

Consequently, increase of feed pressure can affect the diffusivity and solubility of both penetrant in membranes.

Although polymer chain compactness induced by increasing pressure resulted in FFV reduction as well as gases diffusion, but CO_2 with lower kinetic diameter can diffuse more, which leads to higher permeability compared to CH_4.

Alternatively, CO_2 molecules have tendency to pass through membranes via condensation and sorption. Thus, increasing the feed pressure increases the CO_2 concentration in polymer and the plasticization effect of the soluble CO_2 to be enhanced. In consequence the solubility of condensable CO_2 gas in TPX matrix increased by increasing the feed pressure.

Note the intensity of CO_2 permeability increment declined from 8 bar to 10 bar. Increasing pressure up to 10 bar caused the extra compression of the polymer chains, which prevented gas diffusion coefficient and thus reduced intensity of gas permeability increasing.

According to Fig. 6, more increasing permeability of CO_2 compared to the CH_4 due to pressure increasing also can attributed to the polarity of CO_2 gas, which can interact with the polar groups of the polymer properly.

Fig. 7 shows CO_2/CH_4 selectivity of pair gases for the pure TPX membrane and MMMs containing 5, 15 and 30% weight of alumina nanoparticles. According to Fig. 7, the selectivity values of the neat membrane and MMMs increased with increasing feed pressure up to 8 bar. As mentioned earlier, in the pressure of 10 bar the permeability of CO_2 was slightly increased and the more increase in CH_4 permeability at 10 bar led to decrease the pair gases' selectivity.

The selectivity of TPX increased slightly from 7.73 to 8.69 at pressure of 8 bar. In addition, it was found that the CO_2/CH_4 selectivity of MMMs was increased. The CO_2/CH_4 selectivity of MMM with 15 wt% loading of alumina increased from 9.93 at pressure of 2 bar to 11.08 at 8 bar. For 30 wt% loading of alumina (*i.e.*, TPX30) the CO_2/CH_4 selectivity increased from 11.25 at 2 bar to 12.51 at the pressure of 8 bar.

The increase in the permeability and CO_2/CH_4 selectivity of neat TPX and MMMs with increasing the pressure was related to the more complementary condensability as well as more sorption of CO_2. Because of the lower condensability along with less sorption of CH_4, CO_2 permeability increased significantly at higher pressures compared to the permeability of CH_4 and higher selectivity was achieved. A correlation was proposed by Cohen and Turnbull to determine the diffusion coefficient using free volume of polymer as follows [25]:

$$D_i = \alpha \exp\left(\frac{-\gamma v_i}{V_{FV}}\right) \quad (4)$$

where α is a factor that depends on temperature, V_{FV} is average free volume of polymer and γv_i is penetrant size.

According to Eq. (4), increasing the free volume leads to the reduction of the impact of diffusivity selectivity (D_A/D_B) in ideal selectivity. Therefore, solubility selectivity has the main effect on overall selectivity. It means that solubility is a dominant factor due to the increasing in free volume of TPX. In this case, the presence of alumina leads to the higher free volume of membrane. Moreover, sorption of CO_2 increased as pressure increased, and this higher amount of sorption along with higher free volume led to the enhancement of CO_2/CH_4 selectivity [26,27].

Note that usually the selectivity of pair gases reduced as feed pressure increased. In polymeric membranes or MMMs which are comprised from very glassy polymers (i.e., Matrimid, Cellulose acetate, PSF etc.), increasing in feed pressure causes a considerable amount of CO_2 which exposed to the membrane and consequently the great plasticization effect will occur [28,29]. This significant plasticization leads to the increase of polymer chain mobility and thereby the FFV of membrane increases, which enhances the gas diffusion. The selectivity decline is the consequence of this phenomenon [29]. On contrary, TPX has a high free volume naturally and the chain mobility as well as FFV increment made by plasticization has no destructive effect on selectivity of TPX MMMs.

3. Performance of MMMs

Despite the numerous advantages and unique features of polymers, development of polymeric membranes due to inverse relationship between permeability and selectivity was limited to an upper bound. This upper bound and evaluation of the permeability and selectivity was proposed by Robeson [30]. The performance of all synthesized MMMs in CO_2/CH_4 separation compared to Robeson upper bound is shown in Fig. 8 obviously. Fig. 8 confirms that embedded alumina in TPX and higher pressure improves the CO_2/CH_4 selectivity. In addition, the variation of selectivity in terms of CO_2 permeability demonstrates the behavior against the Robeson tradeoff. The high free volume of TPX, more condensability of CO_2, and higher pressure are the main factors affecting the performance of TPX MMMs to overcome the Robeson upper bound. In general, MMMs with high permeability and acceptable selectivity are certainly more striking for industrial application. Considerable increase of CO_2 permeability (from 157.43 Barrer at 2 bar and no loading of Al_2O_3 to 527.78 Barrer at 8 bar and 30 wt% loading of Al_2O_3) and conspicuous enhancement of selectivity (from 7.73 to 12.51) were obtained in TPX MMMs.

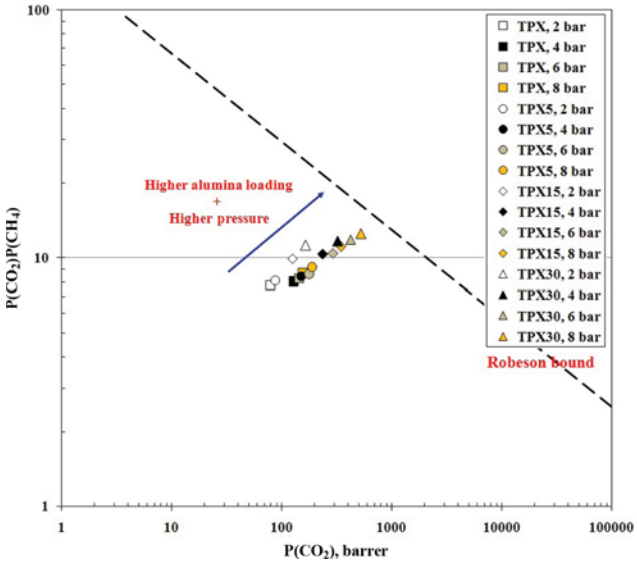

Fig. 8. Performance of TPX and MMMs prepared compared to Robeson upper bound at 2, 4, 6 and 8 bar.

Table 3 illustrates a comparison of the performance of several MMMs. As can be seen, the performance of all MMMs is a strong function of type of additive, based polymer and process conditions. According to the results presented in Table 3, the mixed matrix membranes of TPX with incorporated alumina compared to other MMMs have more permeability. In addition, the prepared TPX/alumina MMMs show proper selectivity values compared with other common glassy polymers. Based on the experimental data obtained in this study, TPX MMMs are a membrane with high permeability values and proper selectivity.

CONCLUSION

The permeability of CO_2 and CH_4 as well as CO_2/CH_4 selectivity in TPX MMMs filled with alumina nanoparticles were evaluated. FT-IR showed that there exist a proper interaction between TPX matrix and alumina. Moreover, TGA results also demonstrated that thermal stability of MMMs increases compared to the neat TPX, due to the high thermal stability of alumina. Furthermore, a uniform dispersion of alumina particles within the TPX matrix without considerable particle agglomeration was observed. Also, CO_2 permeability increased as alumina loading increased in MMMs. Alternatively, the CH_4 permeability was not noticeably improved compared to CH_4 mainly because of the reduction of CH_4 diffusion. The permeability of CO_2 increased from 78.9 Barrer (at no loading of alumina and pressure of 2 bar) to 167.54 Barrer (at 30 wt% of alumina and 8 bar), and the consequent CO_2/CH_4 selectivity

Table 3. A comparison between CO_2/CH_4 separation data for selected MMMs and this work

Polymer	Filler	Loading (wt%)	Operating conditions		P_{CO_2}	P_{CH_4}	P_{CO_2}/P_{CH_4}	Ref.
			Temperature (°C)	Pressure (bar)				
PMP	MIL-53	30	30	2	217.65	11.29	19.28	[3]
PSF	SiO_2	20	35	4.4	19.7	1.1	17.91	[9]
ETPU	SiO_2	15	25	10	8.9	0.31	28.28	[11]
PTMSP	SiO_2	10.2	30	1	1180	180	6.6	[31]
TPX	Al_2O_3	30	25	8	527.78	42.19	12.51	This work

increased from 7.73 to 11.21. Permeability of both gases enhanced as feed pressure increased. The best permeability of gases was obtained at 10 bar. CO_2/CH_4 selectivity in MMMs increased as feed pressure increases from 2 bar to 8 bar. Conversely, the extra increase in feed pressure resulted in selectivity decline.

REFERENCES

1. R. Abedini, S. M. Mousavi and R. Aminzadeh, *Chem. Ind. Chem. Eng. Q.*, **18**, 385 (2012).
2. B. Rahmanian, M. Pakizeh, S. A. A. Mansoori and R. Abedini, *J. Hazard. Mater.*, **187**, 67 (2011).
3. R. Abedini, M. Omidkhah and F. Dorosti, *Iran. J. Polym. Sci. Technol.*, **27**, 337 (2014).
4. M. Arjmandi, M. Pakizeh and O. Pirouzram. *Korean J. Chem. Eng.*, **32**, 1178 (2015).
5. X. Y. Chen, H. Vinh-Thang, D. Rodrigue and S. Kaliaguine, *RSC Adv.*, **3**, 24266 (2013).
6. R. Abedini, S. M. Mousavi and R. Aminzadeh, *Desalination*, **277**, 40 (2011).
7. X. Duan, Y. He, Y. Cui, Y. Yang, R. Krishna, B. Chen and G. Qian, *RSC Adv.*, **4**, 23058 (2014).
8. F. Dorosti, M. Omidkhah and R. Abedini, *Chem. Eng. Res. Des.*, **92**, 2439 (2014).
9. J. Ahn, W. J. Chung, I. Pinnau and M. D. Guiver, *J. Membr. Sci.*, **314**, 123 (2013).
10. M. Valero, B. Zornoza, C. Tellez and J. Coronas, *Micropor. Mesopor. Mater.*, **192**, 23 (2013).
11. Sh. Hassanajili, E. Masoudi, Gh. Karimi and M. A. Khademi, *Sep. Purif. Technol.*, **116**, 1 (2013).
12. Morisato and I. Pinnau, *J. Membr. Sci.*, **121**, 243 (1996).
13. T. Masuda, E. Isobe, T. Higashimura and K. Takada, *J. Am. Chem. Soc.*, **105**, 7473 (1983).
14. R. Abedini, M. Omidkhah and F. Dorosti, *Iran. J. Polym. Sci. Technol.*, **28**, 139 (2015).
15. Z. He, I. Pinnau and A. Morisato, *Desalination*, **146**, 11 (2002).
16. R. Abedini, M. Omidkhah and F. Dorosti, *Int. J. Hydrogen Energy*, **39**, 7897 (2014).
17. R. Abedini, M. Omidkhah and F. Dorosti, *RSC Adv.*, **4**, 36522 (2014).
18. H. Kumazawa, K. Inamori, B. Messaoudi and E. Sada, *J. Membr. Sci.*, **97**, 7 (1994).
19. D. W. Santoshf and P. J. Jyoti, *Polym. Int.*, **53**, 101 (2004).
20. O. Yazici, F. Cakar, O. Cankurtaran and F. Karaman, *J. Appl. Polym. Sci.*, **113**, 901 (2009).
21. S. A. Hosseini, A. Niaei and D. Salari, *Open J. Phys. Chem.*, **1**, 23 (2011).
22. E. J. Samuel and S. Mohanb, *Spectrochim. Acta*, **60**, 19 (2004).
23. H. Zhou, Y. Chen, H. Fan, H. Shi, Z. Lou and B. Shi, *J. Membr. Sci.*, **318**, 71 (2008).
24. A. Jomekian, S. A. A. Mansoori, N. Monirimanesh and A. Shafiee, *Korean J. Chem. Eng.*, **28**, 2069 (2011).
25. M. H. Cohen and D. Turnbull, *J. Chem. Phys.*, **31**, 1164 (1959).
26. F. Dorosti, M. Omidkhah and R. Abedini, *J. Nat. Gas. Sci. Eng.*, **25**, 88 (2015).
27. M. Pakizeh, A. Nezhadmoghaddam, M. R. Omidkhah and M. Namvar Mahboub, *Korean J. Chem. Eng.*, **30**, 751 (2013).
28. A. Ebadi Amooghin, M. Omidkhah and A. Kargari, *J. Membr. Sci.*, **490**, 364 (2015).
29. A. Kılıç, Ç. Atalay-Oral, A. Sirkecioğlu, Ş. B. Tantekin-Ersolmaz and M. G. Ahunbay, *J. Membr. Sci.*, **489**, 81 (2015).
30. L. M. Robeson, *J. Membr. Sci.*, **320**, 390 (2008).
31. K. D. Sitter, P. Winberg, J. D'Haen, C. Dotremont, R. Leysen, J. A. Martens, S. Mullens, F. H. J. Maurer and I. F. J. Vankelecom, *J. Membr. Sci.*, **278**, 83 (2006).